Generation of Novel Building Diaphragm Layouts through Topology Optimization

Astrid W. Fischer[1], James K. Guest[2], Benjamin W. Schafer[3]

[1] Ph.D. Student, Department of Civil Engineering, Johns Hopkins University - Baltimore, MD, USA.
[2] Associate Professor, Department of Civil Engineering, Johns Hopkins University - Baltimore, MD, USA.
[3] Professor, Department of Civil Engineering, Johns Hopkins University - Baltimore, MD, USA.

ABSTRACT

The objective of this paper is to seed innovation in the layout of floor and roof diaphragms in steel buildings. To develop new layouts the optimization of the material distribution has been formulated within an objective function that maximizes the stiffness of the in-plane diaphragm response given a particular volume fraction of material – a classical objective for topology optimization in solid mechanics. A key initial challenge, that is the focus of the work herein, is integrating within the optimization formulation the fact that steel deck has highly orthotropic response: in-plane stiffness is different parallel and perpendicular to the deck profile, and in-plane shear stiffness is lower than the equivalent plate. As a result, the classical 2D topology optimization formulation is expanded to include orthotropic properties and material orientation as design variables. Verification of the formulation is accomplished by examining the in-plane response of a point loaded cantilever. The algorithm is able to successfully maintain response (stiffness) similar (within a few percent) to the isotropic case even when the orthotropic properties are far weaker by optimizing material orientation and placement. Application of the topology optimization algorithm is performed on a large scale diaphragm that has dimensions and constraints consistent with a large steel building under separate study. Significant future challenges remain and are briefly enumerated. This work is part of a larger initiative (steeli.org) that aims to better understand and optimize the role of diaphragms in the seismic response of steel buildings.

Keywords: topology optimization, steel deck, shear stiffness, diaphragm

INTRODUCTION

The seismic resistance of buildings relies on both the vertical and horizontal lateral force resisting systems (LFRS). While much attention has been paid to the design and optimization of the vertical LFRS, comparably little attention has been paid to the horizontal LFRS, or diaphragm. In typical buildings significant mass exists at the floor levels and the diaphragm is responsible for distributing these inertial effects to the vertical LFRS. The multitude of roles the diaphragm may play in successful seismic building performance is summarized in [1]. Today, our understanding and needs for building diaphragms are changing: new design methods and research suggest diaphragms may regularly experience inelastic seismic demands and diaphragm force levels may need to be increased; unique building floor plates require diaphragms with complex shapes and cutouts; new modular buildings require diaphragms with concentrated connection points; and ever increasing demands for efficiency, sustainability, and resilience all lead to a desire to potentially rethink and innovate these systems.

Steel deck diaphragms are a common floor and roof diaphragm typology, and are the motivation for the work here. Examples of bare steel deck and steel deck with concrete fill, as would be common in building roofs and floors respectively, are provided in Figure 1. Within the context of a larger study on steel deck diaphragms [2] a number of 3D steel-framed building archetypes have been designed [3], an example of which is shown in Figure 2. This example employs buckling restrained braces (BRBs) for the vertical LFRS while bare steel deck diaphragms were designed for the roof and composite steel deck with concrete fill diaphragms for the floors. These archetypes provide baseline geometric and material properties for a typical design scenario.

Topology Optimization is a general field that aims to provide optimized layouts of material for a given objective: maximum stiffness, least cost, highest thermal conductivity, etc. [4]. Floor and roof diaphragms are actually dual purpose as they must carry and distribute dead and live load in addition to their diaphragm obligations to provide in-plane shear strength and distribution of lateral forces to the vertical LFRS. Thus in reality, optimized diaphragm topologies are constrained by the need to carry gravity loads and even provide a lower bound stiffness to these transverse loads. Further, seismic performance objectives are realized in the context of dynamic not linear static response and energy dissipation is of interest, therefore investigating the true objective is fully enabled in nonlinear dynamic response. Despite these realities, successful diaphragm designs today use linear static analysis and simplifying assumptions about the load distribution to develop workable solutions.

To provide initial insights on potential innovations we are exploring the application of topology optimization for steel deck diaphragms employing the simple linear static models used in diaphragm design today. However, noting the large difference in deck properties parallel and perpendicular to the corrugations we are interested in allowing the optimization to (a) be orthotropic in nature and (b) allow the optimization to suggest orientation direction for the deck. Developing these two advances is the focus of this work.

Figure 1. Steel deck diaphragms (a) roof - bare deck on open web steel joists [5], (b) floor - concrete filled deck [6]

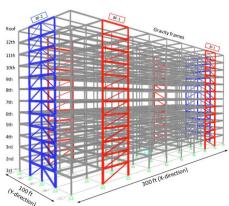Figure 2. Isometric elevation of SDII building archetype with BRB braced frames [3]

TOPOLOGY OPTIMIZATION FORMULATION

The selected objective here is to design bare steel deck diaphragms with maximum stiffness, this is equivalent to the minimum compliance formulation [4] for a 2D continuum problem, using rectangular four node plane stress elements. Minimizing the external work done by the applied loads with an upper bound of available material is expressed as follow:

$$\min_{\rho\ \theta} f = \mathbf{F}^T \mathbf{d}$$
$$s.t. \quad \mathbf{K}\,\mathbf{d} - \mathbf{F} = 0$$
$$\sum_{e\in\Omega} \rho^e\, v^e - V \le 0 \tag{1}$$
$$\rho_{min} \le \rho^e \le 1 \quad \forall\, e \in \Omega$$
$$-\frac{\pi}{2} \le \theta^e \le \frac{\pi}{2} \quad \forall\, e \in \Omega$$

where design variable ρ^e and θ^e are the material concentration (volume fraction) and the material orientation in element e. $\mathbf{F}$ is the applied load vector, $\mathbf{d}$ denotes the nodal displacements, v^e denotes the element volume, the available volume of material in the design domain is denoted V. Finally, the global stiffness matrix $\mathbf{K}$ is assembled from element stiffness matrices $\mathbf{K}^e$:

$$\mathbf{K} = \mathop{A}_{e\in\Omega}\ \mathbf{K}^e(\rho^e, \theta^e) \tag{2}$$

where the element stiffness matrix $\mathbf{K}^e$ is defined for each element as:

$$\mathbf{K}^e(\rho^e, \theta^e) = \rho^e \int_{\Omega^e} \mathbf{B}^{eT}\mathbf{D}^e(\theta^e)\,\mathbf{B}^e\ d\Omega^e \tag{3}$$

in which the strain-displacement matrix is denoted $\mathbf{B}^e$, Ω^e is the element volume domain, and $\mathbf{D}^e$ denotes the element constitutive stiffness matrix, rotated by angle θ^e:

$$\mathbf{D}^e(\theta^e) = \mathbf{R}(\theta^e)^{-1}\ \mathbf{D}_0^{\ e}\ \mathbf{R}(\theta^e)^{-T} \tag{4}$$

The orthotropic material properties at angle $\theta^e=0$ are defined with the constitutive stiffness matrix:

$$\mathbf{D}_{\theta=0}^{\ e} = \frac{1}{1 - v_{12}v_{21}}\begin{bmatrix} E_1 & v_{12}E_2 & 0 \\ v_{21}E_1 & E_2 & 0 \\ 0 & 0 & G\,(1 - v_{12}v_{21}) \end{bmatrix} \tag{5}$$

Where E_α is the Young's modulus for direction 1 and 2, v_α is the Poisson's ratio and the shear stiffness is denoted as G.

The rotation matrix $\mathbf{R}$ in Eq. (4) is defined as [7]:

$$\mathbf{R}(\theta^e) = \begin{bmatrix} \cos(\theta^e)^2 & \sin(\theta^e)^2 & 2\cos(\theta^e)\sin(\theta^e) \\ \cos(\theta^e)^2 & \cos(\theta^e)^2 & -2\cos(\theta^e)\sin(\theta^e) \\ -\cos(\theta^e)\sin(\theta^e) & \cos(\theta^e)\sin(\theta^e) & \cos(\theta^e)^2 - \sin(\theta^e)^2 \end{bmatrix} \tag{6}$$

Sensitivities

The problems in this paper are solved with the gradient based optimizer Method for Moving Asymptotes (MMA) [8]. Therefore the gradients of the objective function f and the constraints computed with respect to the independent design variables ρ and θ. For the minimum compliance problems, the adjoint method [9] is used to calculate the sensitivities of the objective function, to eliminate the derivatives of the displacements:

$$\frac{\partial f}{\partial \rho^i} = -\mathbf{d}^{eT} \frac{\partial \mathbf{K}^e}{\partial \rho^i}(\rho^e, \theta^e)\, \mathbf{d}^e \tag{7}$$

$$\frac{\partial f}{\partial \theta^i} = -\mathbf{d}^{eT} \frac{\partial \mathbf{K}^e}{\partial \theta^i}(\rho^e, \theta^e)\, \mathbf{d}^e \tag{8}$$

Where the element stiffness derivatives with respect to the material density ρ and material orientation θ are:

$$\frac{\partial \mathbf{K}^e}{\partial \rho^i}(\rho^e, \theta^e) = \frac{\partial \rho^e}{\partial \rho^i} \int_{\Omega^e} \mathbf{B}^{eT} \mathbf{D}^e(\theta^e)\, \mathbf{B}^e\ d\Omega^e \tag{9}$$

$$\frac{\partial \mathbf{K}^e}{\partial \theta^i}(\rho^e, \theta^e) = \rho^e \int_{\Omega^e} \mathbf{B}^{eT} \frac{\partial \mathbf{D}^e}{\partial \theta^i}(\theta^e)\, \mathbf{B}^e\ d\Omega^e \tag{10}$$

The derivative of the constitutive stiffness matrix is:

$$\frac{\partial \mathbf{D}^e}{\partial \theta^i}(\theta^e) = \frac{\partial \mathbf{R}(\theta^e)^{-1}}{\partial \theta^i}\, \mathbf{D_0}^e\ \mathbf{R}(\theta^e)^{-T} + \mathbf{R}(\theta^e)^{-1}\ \mathbf{D_0}^e\ \frac{\partial \mathbf{R}(\theta^e)^{-T}}{\partial \theta^i} \tag{11}$$

Material Assumptions/ Diaphragm Stiffness Properties

To ground our analysis to the practical realities of steel deck diaphragms it is important to establish the range of stiffness that is available – i.e. establish the size of the current design space. Bare steel deck diaphragms are particularly interesting since they have a substantial stiffness difference parallel and perpendicular to the corrugation direction. For the purposes of the optimization conducted herein steel deck is transformed into an equivalent orthotropic plate – and thus the range of E_1', E_2', and G' are of primary interest here, where prime signifies the stiffness times plate thickness. The range of stiffness properties for bare steel deck are found with the help of design tables from [10], and [11] which provides a method for calculating the Young's moduli of a corrugated plate. The tables in [10] are extensive and include different deck type; fastener spacing, patterns and types; span lengths; and both bare and filled deck. Considering only the bare steel deck, more than 75,000 layouts are available for the designer with a wide distribution of shear stiffness realized as provided in Figure 3. Bounds on the equivalent material properties are listed in Table 1 along with ratios of the elastic modulus and the shear modulus.
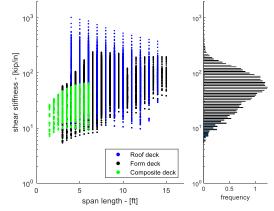

Figure 3. Shear stiffness for bare steel diaphragms

Table 1. Extreme values for the diaphragm Young's moduli and shear stiffness

		min	**max**
E_1'	[kip/in]	694.6	2884.9
	(kN/m)	(121643)	(505223)
E_2'	[kip/in]	0.0264	0.8947
	(kN/m)	(4.623)	(156.69)
G'	[kip/in]	5.4	1017.8
	(kN/m)	(945.68)	(178244)
$\alpha = E_2'/E_1'$		$300 \cdot 10^{-6}$	$1 \cdot 10^{-3}$
$\beta = G'/(E_1'/(2(1+\nu)))$		0.005	1

3

CANTILEVER BEAM EXAMPLE

A classic example in topology optimization is the cantilever beam with tip load [12], as illustrated in Figure 4. This problem is used to verify our implementation of Eq. (1) and explore the impact of material non-dimensional ratios α and β, which define the level of orthotropicity in the solution.

The cantilever beam in this study has dimensions of $L=150$ ft (45.72 m), $h=100$ ft (30.48 m) with a tip load of $F=1$ kip (4.45 kN). The material properties are defined as:

$$E_2 = \alpha \, E_1$$
$$G = \beta \, G_0 \tag{12}$$

where $\alpha<1$ and $\beta<1$ are ratios of the reduction in stiffness from the isotropic material and $G_0 = E_1/(2(1 + \nu_{21}))$, and E_1 denotes the Young's modulus in the strong direction of the material. For the initial example the cantilever beam has the stiffness properties: $E_1=1$, $\nu_{21}=0.3$ and $\nu_{12} = \nu_{21}E_1/E_2=\nu_{21}/\alpha$.

Figure 4. Design domain of cantilever beam example (dimensions selected as ½ the floor plate of Figure 2)

Verification of Code

The problem formulation for the isotropic material case is verified against the "99-line code" [13], optimized solution provided in Figure 5a. Figure 5b illustrates the optimized design produced here using the MMA driver and the formulation of Eq. (1). The mesh is 150x100 plane stress elements and the volume fraction is set to 50%. The optimized objective function evaluation is provided in Figure 5 and the difference is 0.28%. The difference may be attributed to solver choice and tolerance levels and is deemed acceptable.
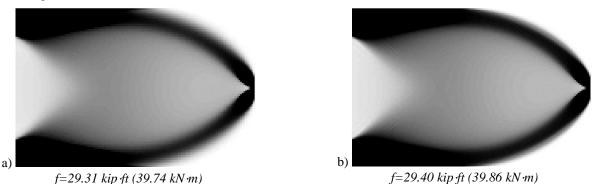

a)   b)

f=29.31 kip·ft (39.74 kN·m)   *f=29.40 kip·ft (39.86 kN·m)*

Figure 5. Optimized structures for isotropic cantilever beam with (a) 99 -line code [13] and (b) MMA and problem formulation of Eq. (1)

Optimized Design for Fixed Angles

In the following we explore the impact of two changes consistent with steel deck diaphragms: (1) variation in α, i.e. reduced E_2 compared to E_1, and (2) variation in β, i.e. reduced G compared with its isotropic equivalent. In addition, we also consider the unique impact of overall orientation, θ, on the solution. For these solutions a 60x40 mesh of plane stress elements, and a volume fraction of $V=50\%$ are maintained. The initial starting condition is an even material density of $\rho=0.5$. For each case considered we may compare the change in the objective function (ratio of tip displacement) after optimization with that arrived

at from the isotropic case as provided in Figure 6. In addition, the final optimized topologies are provided for selected cases in Figure 7-9.

The impact of α and θ is provided in Figure 6a. Having E_1 perpendicular to the loading (θ) always provides the stiffest solution for the cantilever problem regardless of α (i.e. reduced E_2). Interestingly, for the $\theta=0°$ case the optimized displacement converges to a constant value as E_2 reduces. The explanation for this behavior may be found in Figure 7c which demonstrates that the optimized design of a cantilever beam with almost no stiffness in the vertical direction is a solid beam that uses the upper and lower fibers in tension and compression to withstand the vertical load at the tip. The weakest solutions (Figure 6a) occur when the strong (E_1) direction is vertical ($\theta=90°$). Figure 8 provides the optimized designs, which are dominated by the shear strength of the material.

a)   b)

Figure 6. Change in overall diaphragm stiffness as (a) the stiffness ratio increases and (b) shear stiffness increases

a)   b)   c)

  f=36.84 kip·ft (49.92 kN·m)   *f=221.45 kip·ft (300.25 kN·m)*   *f=1539.02 kip·ft (2086.63 kN·m)*

Figure 7. Optimized design for the cantilever beam example for fixed angle $\theta=0°$, $\beta=1$, and decreasing Young's modulus by a factor of (a) $\alpha=0.1$, (b) $\alpha=10^{-3}$, and (c) $\alpha=10^{-6}$.

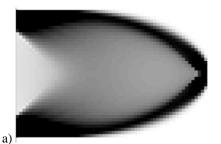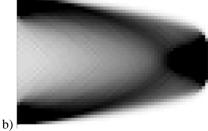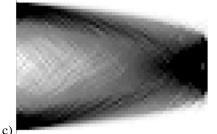a)   b)   c)

  f=171.96 kip·ft (233.15 kN·m)   *f=1478.44 kip·ft (2004.49 kN·m)*   *f=81155.77 kip·ft (110032.40 kN·m)*

Figure 8. Optimized design for the cantilever beam example for fixed angle $\theta=90°$, $\beta=1$, and decreasing Young's modulus by a factor of (a) $\alpha=0.1$, (b) $\alpha=10^{-2}$, and (c) $\alpha=5\cdot10^{-5}$.

The impact of β (reduced shear stiffness) and θ is provided in Figure 6b, since $E_1=E_2$ ($\alpha=1$) the impact of material orientation should be negligible. The small differences between the different orientations is believed to be caused by numerical sensitivity when β becomes less than ~0.1. Selected optimized topologies are provided in Figures 9.
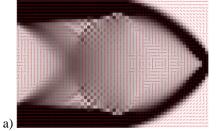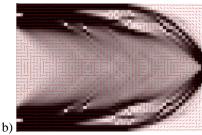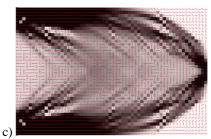
f=38.45 kip·ft (52.13 kN·m)   *f=184.51 kip·ft (250.16 kN·m)*   *f=1591.87 kip·ft (2158.28 kN·m)*

Figure 9. Optimized design for the cantilever beam example for fixed angle θ=0°, α=1, and decreasing shear modulus by a factor of (a) β=0.5, (b) β=0.05, and (c) β=0.005.

Optimized Design with Design Variable ρ and θ

The formulation presented in Eq. (1)-(11) uses two design variables per element: ρ^e and θ^e. In Figure 10 and 11 we have provided the fully optimized topologies for different levels of α and β. For each element material orientation, θ^e, is depicted as a short red line in the E_1 direction, and element density, ρ^e, by grayscale with black $\rho^e=1$. Results as E_2 decreases in relation to E_1 (varied α) provided in Figure 10 indicate that the solution may maintain stiffness very near the isotropic case even with low α. With free material orientation, the cantilever beam can preserve its global stiffness when one of the material stiffnesses significantly reduces. Figure 11 provides similar results for the case when the shear stiffness is reduced (varied β). Notably, change in material orientation plays a stronger role in the solution of Figure 11, as the material orientation must provide the load path when the shear stiffness is lost. We note in these solutions the presence of subtle checkerboard patterns or one-node chain features, which are known in topology optimization to appear when using low-order finite elements with isotropic material properties [14]. These can be circumvented using more sophisticated topological representations, such as to control the length scale of designed features [12-15].
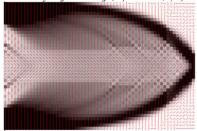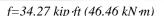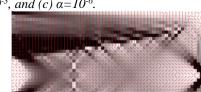

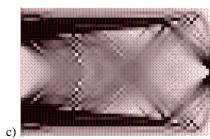*f=30.65 kip·ft (41.56 kN·m)*   *f=30.69 kip·ft (41.61 kN·m)*   *f=30.20 kip·ft (40.95 kN·m)*

Figure 10. Optimized design for the cantilever beam example for starting angle θ=0°, β=1 and decreasing Young's modulus by a factor of (a) α=0.1, (b) α=10⁻³, and (c) α=10⁻⁶.

f=34.27 kip·ft (46.46 kN·m)   *f=49.12 kip·ft (66.60 kN·m)*   *f=41.66 kip·ft (56.48 kN·m)*

Figure 11. Optimized design for the cantilever beam example for starting angle θ=0°, α=1 and decreasing shear modulus by a factor of (a) β=0.5, (b) β=0.05, and (c) β=0.005.

DIAPHRAGM EXAMPLE

To illustrate the potential of the developed and verified topology optimization algorithm consider a diaphragm motivated by [3] (Figure 2) as illustrated in Figure 12: The supports on the short sides are at the location of the BRB braced frames, loads are applied uniformly on each side to simulate a uniform inertial force acting on the floor, and is set to $p=0.5$ kip/ft (7.30 kN/m). The material properties are: $E_2'=10.73$ kip/ft (156.59 kN/m), $G'=12213$ kip/ft (178.24 MN/m), and $E_1'=34618$ kip/ft (505.22 MN/m) and dimensions are $L=150$ ft (45.72 m), $h=100$ ft (30.48 m). The volume fraction is set to 50%. For the initial conditions an even material density distribution of $\rho^e=0.5$ and material orientation $\theta=0°$ are used.

The resulting optimized solution is provided in Figure 13 and has several notable features. First, consistent with intuition the chords (material on the long sides of the building) are prominent and oriented with the strong direction parallel to the long side. Second, the optimized topology does not use traditional collectors (material on the short side of the building) instead material is channeled to a large node that connects to the supports and employs an orientation largely parallel to the short side of the building. Between these large collector nodes and the chords the topology favors struts with an angled material orientation. Realizing such complex geometries in practice would be challenging in steel diaphragm systems – but the optimization points to the potential benefits of re-thinking the manner in which forces are brought to the chords and collectors and further refinements will be sought to bring greater practicality to the final solutions.
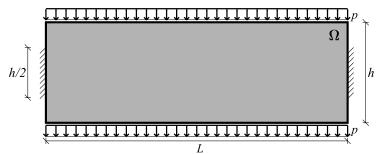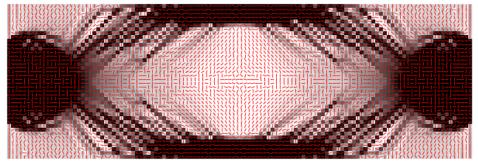

Figure 12. Layout of diaphragm example inspired from the SDII archetype layout [3]

f=9.24 kip·ft (12.53 kN·m)

Figure 13. Optimized design of diaphragm example

CONCLUSIONS

Motivated by the directional nature of bare steel deck stiffness and an interest in exploring innovative and efficient diaphragm solutions we developed a two-dimensional topology optimization algorithm that is inclusive of orthotropic material properties and allows material orientation to be a design variable. We verified the algorithm on a classic cantilever problem, widely employed in topology optimization. It was found that decreasing one of the Young's moduli or the shear stiffness while fixing the material orientation will significantly decrease the cantilever beam's overall stiffness compared to the isotropic case. However, when the optimizer can decide the orientation of the material for each element, it was found that the beam can nearly maintain its isotropic stiffness even as one of the Young's moduli or the shear stiffness reduces. A final example was provided for a large diaphragm in an example building where the optimization reveals new ideas about how to distribute in-plane stiffness for efficient distribution of inertial load from the floor to the braced frames. Significant future work remains: impact of new layouts, consideration of steel deck with concrete fill properties, integration of more practical constructability constraints, integration of gravity load constraints, incorporation of cost, etc. Despite the large degree of future work remaining, the paper introduces the potential of topology optimization to provide new insights for the design of building diaphragms.

ACKNOWLEDGMENTS

REFERENCES

[1] S. Easterling, R. Sabelli and T. Sabol, "Seismic Design of Composite Steel Deck and Concrete-filled Diaphragms - A Guide for Practicing Engineers," NEHRP Seismic Design Technical Brief No. 5, NIST GCR 11-917-10, 2018.

[2] S. Easterling, M. Eatherton, J. Hajjar, R. Sabelli and B. Schafer, "Steel Diaphragm Innovation Initiative," 29 January 2019. [Online]. Available: steeli.org.

[3] S. Torabian, M. Eatherton, W. Easterling, J. Hajjar and B. Schafer, "SDII Building Archetype Design v1.0," CFSRC Report R-2017-04, permanent link: jhir.library.jhu.edu/handle/1774.2/4063, 2017.

[4] M. Bendsøe and O. Sigmund, "Topology Optimization - Theory, Methods and Applications," Springer Verlag, 2002.

[5] ASC, "Roof Deck Design Guide," ASC Steel Deck, v1.0,, 2018.

[6] ASC, "Composite Deck and Non-Composite Deck for Floor and Roof Deck Applications," ASC Steel Deck, v1.0, 2018.

[7] A. Gaynor, J. Guest and C. Moen, "Reinforced concrete force visualization and design using bilinear truss-continuum topology optimization," ASCE Journal of Structural Engineering, 139(4): 607-618, 2013.

[8] K. Svandberg, "The method of moving asymptotoes—a new method for structural optimization," Int. J. Numer. Methods Eng., 24, 359–373, 1987.

[9] J. Guest and T. Igusa, "Structural optimization under uncertain loads and nodal locations," Computer Methods in Applied Mechanics and Engineering, 198(1), 116-124, 2008.

[10] L. Luttrell, "Diaphragm Design Manual, fourth edition," Steel Deck Institute, 2015.

[11] Y. Xia and M. Friswell, "Equivalent Models of Corrugated Panels," International Journal of Solids and Structures, 49, 1453-1462, 2012.

[12] J. Guest, J. Prevost and T. Belytschko, "Achieving minimum length scale in topology optimization using nodal design variables and projection functions," International Journal for Numerical Methods in Engineering, 61(2): 238 – 254, 2004.

[13] O. Sigmund, "A 99 line topology optimization code written in Matlab," Struct Multidisc Optim, 21, 120-127, 2001.

[14] O. Sigmund and J. Petersson, "Numerical instabilities in topology optimization: A survey on procedures dealing with checkerboards, mesh-dependencies and local minima," *Structural optimization,* vol. 16, no. 1615-1488, pp. 68--75, 1998.

[15] J. Guest, A. Asadpoure and S. HA, "Eliminating beta-continuation from Heaviside projection and density filter algorithms," Structural and Multidisciplinary Optimization, 44(4): 443-453, 2011.